Letter | Editors' Suggestion

Possible $s_{\pm}$-wave superconductivity in $La_3Ni_2O_7$

Qing-Geng Yang,[1] Da Wang,[1,2,*] and Qiang-Hua Wang[1,2,†]

[1]*National Laboratory of Solid State Microstructures and School of Physics, Nanjing University, Nanjing 210093, China*

[2]*Collaborative Innovation Center of Advanced Microstructures, Nanjing 210093, China*

(Received 15 June 2023; revised 30 August 2023; accepted 2 October 2023; published 17 October 2023)

Recently, the bulk nickelate $La_3Ni_2O_7$ is reported to show a signature of high-temperature superconductivity under high pressure above 14 GPa [H. Sun *et al.*, Nature (London) **621**, 493 (2023)]. We analyze the pairing mechanism and pairing symmetry in a bilayer Hubbard model with two orbitals in the E_g multiplet. In the weak to moderate interaction regime, our functional renormalization group (FRG) calculations yield $s_{\pm}$-wave Cooper pairing triggered by leading spin fluctuations. The gap function changes sign across the Fermi pockets, and in real space the pairing is dominated by intra-unit-cell intraorbital components with antiphase between the on-site ones. In the strong-coupling limit, we develop a low-energy effective theory in terms of atomic one- and two-electron states in the E_g multiplet. The variational treatment of the effective theory produces results consistent with the FRG ones, suggesting the robustness of such a pairing function. The driving force for superconductivity in the strong-coupling limit can be attributed to the local pair-hopping term and the spin exchange on vertical bonds. We also discuss a possible scenario for the weak insulating behavior under low pressures in terms of the tendency toward the formation of charge order in the strong-coupling limit.

DOI: 10.1103/PhysRevB.108.L140505

Introduction. After the discovery of cuprate high-T_c superconductors [1,2], there are continuing efforts to search for superconductivity in perovskites of similar structure, such as ruthenates [3], cobaltates [4], and nickelates [5], in order to understand how unique the copper is in cuprates on the one hand, and to discover new families of high-T_c superconductors, on the other hand. As a possible breakthrough along this line, a recent report shows a signature of superconductivity in the bulk nickelate $La_3Ni_2O_7$ with T_c as high as 80 K at a pressure above 14 GPa [6]. It has a bilayer perovskite structure with the nickel atom sitting in the center of each oxygen octahedron, with a layered NiO_2 plane similar to the CuO_2 plane in cuprates. However, the valence of a Ni atom fluctuates between Ni^{2+} and Ni^{3+}, with an average $3d^{7.5}$ atomic configuration. Under high pressure, both $3d_{x^2-y^2}$ and $3d_{3z^2-r^2}$ orbitals in the E_g multiplets are active near the Fermi level [6,7]. The E_g multiplet in $La_3Ni_2O_7$ is also different from the t_{2g} multiplet in iron-based superconductors [8,9] where the Fe atom is in an edge-sharing tetrahedron. At the fractional filling, $La_3Ni_2O_7$ is unlikely to form a Mott insulator. But quite unexpectedly, the material is weakly insulating at lower pressures [6].

The novel attributes of $La_3Ni_2O_7$ motivate us to explore the pairing mechanism and pairing symmetry therein, and to understand the weak insulating behavior under lower pressures. We perform the analysis within a bilayer two-orbital Hubbard model by functional renormalization group (FRG) in the the weak to moderate interaction regime, and effective theory in the strong-coupling limit. We find the Cooper pairing has $s_{\pm}$-wave symmetry. In momentum space, the sign change of the gap function is compatible with the structure of leading spin fluctuations, suggesting pairing triggered by spin fluctuations. In real space, the Cooper pair is dominated by intraorbital pairing on site and on the vertical interlayer bond, with stronger amplitudes in the $d_{3z^2-r^2}$-orbital content, antiphase between the on-site pairs. In the strong-coupling limit, we develop a low-energy effective theory in terms of atomic one- and two-electron states in the E_g multiplet. The results from variational treatment of the effective theory are consistent with the FRG results. The driving force for superconductivity in the strong-coupling limit can be attributed to the local pair-hopping interaction and the spin exchange of $d_{3z^2-r^2}$ electrons on vertical bonds. We also discuss a possible scenario of the weak insulating behavior under lower pressures in terms of the tendency toward charge ordering in the strong-coupling limit.

Model. We start from a two-orbital ($d_{3z^2-r^2}$ and $d_{x^2-y^2}$) tight-binding model on a bilayer square lattice as extracted from the Wannier fitting to the band structure of density functional theory (DFT) [7],

$$H_0 = \sum_{i\delta,ab,\sigma} t_{\delta}^{ab} c_{ia\sigma}^{\dagger} c_{i+\delta b\sigma} + \sum_{ia\sigma} \varepsilon_a c_{ia\sigma}^{\dagger} c_{ia\sigma}, \tag{1}$$

where t_{δ}^{ab} is the hopping matrix element between the a orbital on site i and the b orbital on site $i+\delta$, σ denotes spin, and ε_a is the on-site energy of the a orbital. Up to C_{4v} symmetry, the tight-binding parameters are given by $(t_{100}^{xx}, t_{110}^{xx}, t_{00\frac{1}{2}}^{xx}, t_{100}^{zz}, t_{110}^{zz}, t_{00\frac{1}{2}}^{zz}, t_{100}^{xz}, t_{10\frac{1}{2}}^{xz}, \varepsilon_x, \varepsilon_z) = (-0.483, 0.069, 0.005, -0.110, -0.017, -0.635, 0.239, -0.034, 0.776, 0.409)$ eV [7]. Here x/z denotes the $d_{x^2-y^2}/d_{3z^2-r^2}$ orbital, and the vertical interlayer distance is assigned as $\frac{1}{2}$.

*dawang@nju.edu.cn
†qhwang@nju.edu.cn

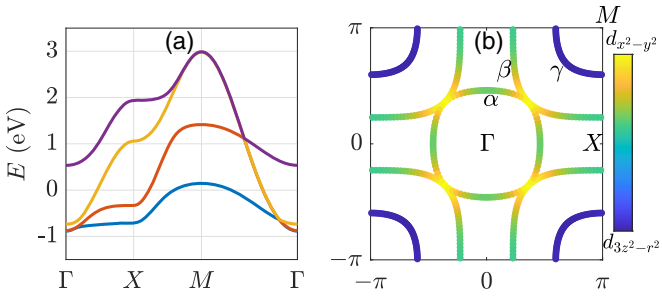

FIG. 1. (a) Band dispersion along the high-symmetry lines Γ-X-M-Γ. (b) Fermi surfaces in the Brillouin zone with color-scaled orbital characters. The three pockets are labeled by α, β, and γ, respectively.

We note that the hopping of the $d_{3z^2-r^2}$ electron along the vertical interlayer bond is the strongest.

The energy bands (a) and Fermi surfaces (b) are shown in Fig. 1. There are three bands crossing the Fermi level, leading to three Fermi pockets: one electronlike α pocket around Γ, one small holelike γ pocket around M, and another large holelike β pocket around M. From the color scale in Fig. 1(b), both the α and β pockets show strong orbital hybridizations, while the γ pocket mainly comes from the $d_{3z^2-r^2}$ orbital. From the DFT calculations, the shallow γ pocket only appears in the high-pressure phase, while it vanishes in the low-pressure phase [6], suggesting its importance for superconductivity in this material.

We consider the multiorbital atomic Coulomb interactions

$$H_I = \frac{1}{2}\sum_{i,a\neq b,\sigma\sigma'}(U' n_{ia\sigma}n_{ib\sigma'} + J_H c^\dagger_{ia\sigma}c_{ib\sigma}c^\dagger_{ib\sigma'}c_{ia\sigma'}) + \sum_{ia} U n_{ia\uparrow}n_{ia\downarrow} + \sum_{i,a\neq b} J_P c^\dagger_{ia\uparrow}c^\dagger_{ia\downarrow}c_{ib\downarrow}c_{ib\uparrow}, \quad (2)$$

where U is the intraorbital Hubbard repulsion, U' is the interorbital Coulomb interaction, J_H is the Hund's coupling, and J_P is the pair-hopping interaction. Throughout this work, we use the Kanamori relations [10] $U = U' + 2J_H$ and $J_H = J_P$.

Functional renormalization group. We first perform the singular-mode functional renormalization group (SM-FRG) [11,12] calculations to look for possible electronic instabilities in the system. The FRG approach is controlled in the weak to moderate interaction regime [13–16]. It provides the flow of the effective interactions between quasiparticles versus a running infrared cutoff energy scale Λ (the lowest Matsubara frequency in our case). In our SM-FRG, we define a fermion bilinear $c^\dagger_{a\sigma}(\mathbf{R})c^\dagger_{b\sigma'}(\mathbf{R}+\delta)$ in the pairing channel, labeled by the orbital-spin combination $(a\sigma, b\sigma')$ and the internal displacement δ, in addition to the shared position $\mathbf{R}$. Similar bilinears can be defined in the particle-hole channels, and are transformed into the momentum space in the calculations. As Λ is lowered from the ultraviolet limit, we extract from the full effective interactions the scattering matrices $V_{\mathrm{SC,SDW,CDW}}(\mathbf{q})$ between fermion bilinears (of momentum $\mathbf{q}$) in the superconducting (SC), spin-density-wave (SDW) and charge-density-wave (CDW) channels, respectively. We monitor the flow of the leading negative eigenvalue S in each channel. The first

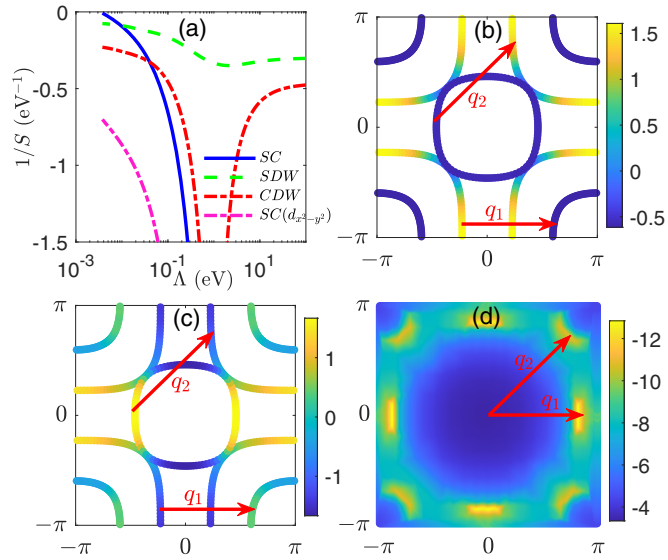

FIG. 2. (a) FRG flow of the leading eigenvalues S (plot as $1/S$) versus the running energy scale Λ in the SC, SDW, and CDW channels, for $(U, J_H) = (3, 0.3)$ eV. For comparison, the subleading eigenvalue in the pairing channel is also plotted. (b) and (c) show the leading s-wave and subleading $d_{x^2-y^2}$-wave gap functions on the Fermi surfaces (color scale). (d) shows the renormalized interaction $V_{\mathrm{SDW}}(\mathbf{q})$ when the SC channel diverges. The two arrows indicate two dominant scattering momenta $\mathbf{q}_{1,2}$, which connect Fermi points with opposite gap signs as seen in (b) and (c).

divergence at a critical scale $\Lambda = \Lambda_c$ signals an emerging electronic order at transition temperature $T_c \sim \Lambda_c$, described by the bilinear combination in the eigen scattering mode of the diverging channel. The technical details of our SM-FRG can be found in the Supplemental Material [17] and Refs. [11,18,19].

A typical FRG flow is shown in Fig. 2(a), where we plot $1/S$ versus Λ for the case of $(U, J_H) = (3, 0.3)$ eV. The SDW channel is strongest at high energy scales, as in the bare interaction. The CDW channel is initially reduced by Coulomb screening, which also causes the SDW channel to decrease slightly. The SC channel does not show up initially since it is repulsive. The SDW channel begins to increase further as $\Lambda \sim 1$ eV, as off-site spin correlations are induced. Meanwhile, through the channel overlap, the SDW channel triggers the rise of the SC channel. This is a manifestation of the well-known Kohn-Luttinger mechanism [20]. The CDW also rises because off-site bilinears (such as the valence bond) in this channel can be induced by SDW. As Λ is lowered further, the SDW and CDW channels tend to saturate because the phase space for low-energy particle-hole excitations decreases. However, the SC channel at zero bilinear momentum $\mathbf{q} = 0$ can continue to rise through the Cooper mechanism. Finally the SC channel diverges first, suggesting an instability of the normal state toward the SC state.

We next analyze the pairing function. It can be obtained directly from the leading eigenmode of the SC-channel interaction $V_{\mathrm{SC}}(\mathbf{q} = \mathbf{0})$ in the fermion bilinear basis (see the Supplemental Material [17] for more details). The eigenmode corresponds to a pairing term $H_{SC} = \sum_{i\delta,ab}\Delta^{ab}_\delta c^\dagger_{ia\uparrow}c^\dagger_{i+\delta b\downarrow}$, and

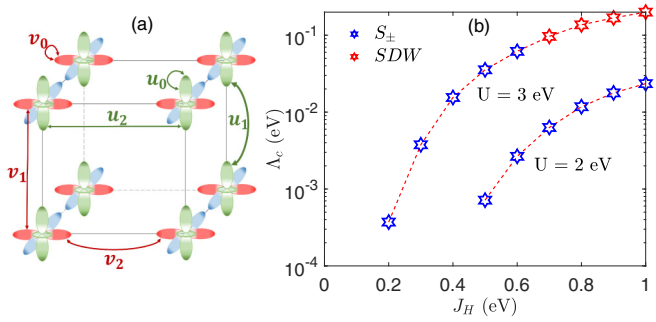

FIG. 3. (a) Schematic plot of the dominant intraorbital pairing components in real space, with $u_{0,1,2}$ for $d_{3z^2-r^2}$ orbitals (vertical rods) and $v_{0,1,2}$ for $d_{x^2-y^2}$ orbitals (planar crosses), up to translation and C_{4v} symmetry. (b) The critical scale Λ_c versus J_H for two values of U. Blue and red stars stand for $s_\pm$-wave SC and SDW, respectively.

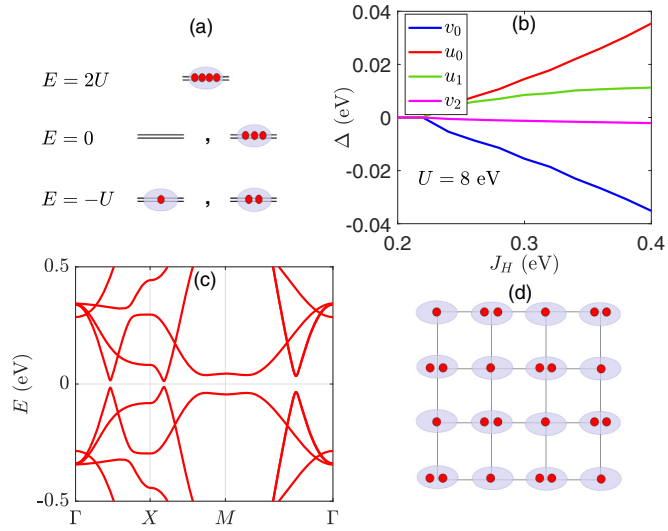

FIG. 4. (a) Atomic charge states and energy levels for 3/2-filling. (b) Pairing components in H_v versus J_H at $U = 8$ eV. (c) Band structure using H_v for $(U, J_H) = (8, 0.3)$ eV. (d) A schematic plot of the possible in-plane CDW at lower pressures.

the dominant pairing components are illustrated in Fig. 3(a), where $u_{0,1,2}$ denotes Δ_δ^{zz}, and $v_{0,1,2}$ denotes Δ_δ^{xx}. In the case of $(U, J_H) = (3, 0.3)$ eV and up to a global scale, (i) the pairing within the $d_{3z^2-r^2}$ orbital is $u_0 = -0.43$ (on site) and $u_1 = 0.51$ (on the vertical bond); (ii) the pairing between the $d_{x^2-y^2}$ orbitals is $v_0 = 0.14$ (on site) and $v_1 = 0.07$ (on vertical bond); and (iii) the intraorbital pairing on in-plane nearest-neighbor bonds is $(u_2, v_2) \sim (-0.05, -0.02)$ for $d_{3z^2-r^2}$ and $d_{x^2-y^2}$ orbitals, respectively. The pairing between the $d_{3z^2-r^2}$ orbitals is much stronger. The antiphase between u_0 and v_0 is consistent with the repulsive bare local pair-hopping interaction J_P. The pairing symmetry is clearly s wave.

To gain more insights, we further project the pairing function into the band basis to obtain the gap function $\Delta_{n\mathbf{k}} = \langle n\mathbf{k}| \sum_\delta \Delta_\delta e^{i\mathbf{k}\cdot\delta} |n\bar{\mathbf{k}}\rangle$ where $|n\mathbf{k}\rangle$ is the Bloch state for band n, Δ_δ is understood as a matrix in the orbital-sublattice basis, and we have used the time-reversal symmetry $|n\bar{\mathbf{k}}\rangle = T|n\mathbf{k}\rangle$ (for $\bar{\mathbf{k}} = -\mathbf{k}$) to simplify the expression. The gap function (color scale) is shown on the Fermi surfaces in Fig. 2(b). Both α and γ pockets are fully gapped with the same sign, while the gap on the β pocket is largely of opposite sign and diminishes in the nodal direction where the two pockets are very close. Therefore, exactly speaking, the pairing symmetry is $s_\pm$ wave, similar to the case in iron pnictides [21], bilayer Hubbard models [22–24], and infinite layer nickelates [25]. On the other hand, we note that as the leading eigenmode diverges, the subleading one with $d_{x^2-y^2}$ pairing is finite [see Fig. 2(a)] and can be ruled out as a competitor for the SC state. However, for comparison, we also plot its gap function in Fig. 2(c). Since the γ pocket is near M, the $d_{x^2-y^2}$-wave gap function is nodal, and tiny on the entire γ pocket. This should be unfavorable to gain condensation energy if such a pairing would occur in the SC state. Interestingly, the experiment shows that the SC phase appears when the γ pocket appears [6]. This fact supports our $s_\pm$ wave instead of $d_{x^2-y^2}$ wave as the leading pairing symmetry.

In Fig. 2(d), we plot the leading negative eigenvalue of the renormalized $V_{\mathrm{SDW}}(\mathbf{q})$ in the momentum space as the pairing channel diverges. We see the spin interaction is strong near momenta $\mathbf{q}_1 \sim (0.75, 0.75)\pi$ and $\mathbf{q}_2 \sim (0.84, 0)\pi$, up to symmetry-related images, which appear to connect the Fermi points where the gap function has opposite signs, as seen from the same arrows in Figs. 2(b) and 2(c). This is consistent with pairing triggered by spin fluctuations, as the FRG flow already suggests. A similar mechanism is believed to work in cuprates and iron pnictides, at least in the weak-coupling scenario [26].

To see the robustness of the $s_\pm$-wave pairing, we performed systematic calculations by varying J_H and U, with $J_H \leqslant U/2$. Figure 3(b) shows the phase diagram. We find the $s_\pm$-wave pairing is always favored, and the critical scale increases with J_H, until the SDW channel begins to win for larger U and J_H. The reason is the SDW interaction is enhanced by J_H, even at the bare level. While the exact values for U and J_H are unavailable at this stage, our results show that the SC phase is realized in a large regime of the parameter space.

Strong-coupling limit. We first assume $U = U', J_H = J_P = 0$, and ignore the small crystal field splitting and the kinetic hopping. (The difference to this situation will be taken as perturbations.) In the atomic limit, the one-electron ($1e$) and two-electron ($2e$) states on a site are degenerate if the chemical potential is set at $\mu = U$. The energy levels for all possible atomic charge states is illustrated in Fig. 4(a). The ground state manifold is spanned by the $1e$ and $2e$ states, and the density of both atomic states should be 1/2 to match the average electron filling level 3/2. Then up to the second order in the small perturbations, the effective Hamiltonian in the low-energy sector can be written as

$$\begin{aligned}\tilde{H} = &\sum_{\langle ij\rangle a,b,\sigma} \left(t_{ij}^{ab} c_{ia\sigma}^\dagger c_{jb\sigma} Q_{1e,i} Q_{2e,j} + \mathrm{H.c.}\right) \\ &+ \sum_{\langle ij\rangle a,n=1,2} J_{ij}^a \left(\mathbf{S}_{ia}\cdot\mathbf{S}_{ja} - \frac{1}{4} n_{ia} n_{ja}\right) Q_{ne,i} Q_{ne,j} \\ &+ \sum_{i,a} J_H (Q_{2e,ia} - Q_{1e,ia} Q_{1e,i\bar{a}}) \\ &+ \sum_{i,a>b} J_H \left(\frac{1}{4} n_{ia} n_{ib} - \mathbf{S}_{ia}\cdot\mathbf{S}_{ib}\right) Q_{1e,ia} Q_{1e,ib}\end{aligned}$$

$$+\sum_{i,a>b} J_P(c^\dagger_{ia\uparrow}c^\dagger_{ia\downarrow}c_{ib\downarrow}c_{ib\uparrow} + \text{H.c.})$$
$$+\sum_{ia}\epsilon_a(Q_{1e,ia}+2Q_{2e,ia}). \quad (3)$$

This can be taken as a generalized two-orbital t-J model, but with the important difference that double occupancy is allowed. To be more specific, for a given site i, $Q_{ne,ia}$ is a projection operator for charge ne on the a orbital, $\mathbf{S}_{ia}$ for spin operator, and $Q_{ne,i}$ for total charge ne at site i. The second line is the superexchange by second-order hopping processes via an intermediate atomic $3e$ or $0e$ state of energy $\bar{U} \sim (U + U')/2 = U - J_H$, resulting in the antiferromagnetic coupling $J^a_{ij} \sim 4(t^{aa}_{ij})^2/\bar{U}$. Note we ignored superexchange processes involving t^{ab}_{ij} or $t^{aa}_{ij}t^{bb}_{ji}$ with $a \neq b$, since they are much smaller than the leading orbital-diagonal cases. In the third line, $\bar{a}$ denotes the orbital other than a, and in the last line we subtracted the average of the crystal field to write $\epsilon_a = \varepsilon_a - \bar{\varepsilon}$. On the other hand, we dropped a constant U (per site), which is the largest energy scale we designed to eliminate. The Hamiltonian acts on a many-body state under a global projection operator $P = P_{N_e}\Pi_i(Q_{1e,i} + Q_{2e,i})$, where P_{N_e} is a projection operator for the total charge, $\sum_i(Q_{1e,i} + 2Q_{2e,i}) = N_e$.

As the usual one-band t-J model, the above model still contains strong correlation effects due to the projection operators and constraints. We proceed to investigate the (uniform paramagnetic) ground state $|G\rangle$ by variational principle: $|G\rangle = P|0\rangle$, where $|0\rangle$ is the ground state of a variational free Hamiltonian,

$$H_v = \textstyle\sum_{ijab\sigma}\left[h^{ab}_{ij}c^\dagger_{ia\sigma}c_{ja\sigma} + \sigma\left(\Delta^{ab}_{ij}c^\dagger_{ia\sigma}c^\dagger_{jb\bar{\sigma}} + \text{H.c.}\right)\right],$$

where h's describe hopping on bonds as well as on-site energy and orbital hybridization, and Δ's are the corresponding singlet pairing amplitudes. The energy $E = \langle G|\tilde{H}|G\rangle/\langle G|G\rangle$ needs to be minimized by optimizing the variational parameters in H_v. This could be performed by variational Monte Carlo, but for a flavor of the underlying physics, we perform the minimization semianalytically in the Gutzwiller approximation [27,28]. See Supplemental Material [17] for details. The variational calculation always ends up with intraorbital s-wave singlet pairing, with dominant real-space components as schematically shown in Fig. 3(a). The numerical value is shown in Fig. 4(b) for these components versus J_H for $U = 8$ eV. The two on-site intraorbital components u_0 and v_0 are large and always antiphase, increasing with J_H, the component u_1 on vertical bond for $d_{3z^2-r^2}$-orbital is subleading, while the other components are much weaker. This demonstrates that our FRG results obtained for weaker interactions are robust and suggestive even for the strong-coupling case. Moreover, we find if we switch off the J_P term in Eq. (3), then $(u_0, v_0) \to 0$ and only u_1 survives and is also small. This shows that the driving force for pairing in the strong-coupling limit is the local pair-hopping interaction and spin exchange of $d_{3z^2-r^2}$ electrons on vertical bonds. Figure 4(c) shows the Bogoliubov–de Gennes band structure using H_v. Clearly, the gap opens along the entire line cuts, consistent with the s-wave symmetry. We also checked that the normal state part of H_v leads to a bandwidth that is roughly a half of the unprojected one. We should point out the above theory applies best for smaller values of J_H. A larger J_H may eventually drive the system into magnetic ground states [29].

Finally, we recall that in a usual one-band Hubbard model on the square lattice, the nearest-neighbor Coulomb interaction V would favor a charge-ordered state provided that $V > U/4$ [30]. However, in the above projected Hamiltonian suitable for the average 3/2-filling, the $1e$ and $2e$ states are near degenerate at the atomic level, so that U does not hamper the charge ordering of the $1e$ and $2e$ states. In fact, it is advantageous to form a staggered charge order of $1e$ and $2e$ states on the lattice, a form of Wigner crystal [see Fig. 4(e)], to save Coulomb energy. The charge order only has to fight against the kinetic quantum fluctuations, and would set in once $4V\chi_c \geqslant 1$ in the simple Stoner picture, where χ_c is the charge susceptibility. In the present case, the projection reduces the bandwidth and enhances the charge susceptibility. More interestingly, at lower pressures the bare bandwidth is smaller, so that the charge order is more likely to occur. The charge order reduces the charge mobility and the transition may be first order. This may explain the weak insulating behavior at lower pressures, and the abrupt emergence of the SC state at higher pressures [6], in addition to the effect of possible aptical oxygen vacancies.

Acknowledgments. This work is supported by National Key R&D Program of China (Grant No. 2022YFA1403201) and National Natural Science Foundation of China (Grants No. 12374147, No. 12274205, and No. 11874205).

[1] J. G. Bednorz and K. A. Muller, Possible high T_c superconductivity in the Ba-La-Cu-O system, Z. Phys. B **64**, 189 (1986).
[2] P. A. Lee, N. Nagaosa, and X.-G. Wen, Doping a Mott insulator: Physics of high-temperature superconductivity, Rev. Mod. Phys. **78**, 17 (2006).
[3] Y. Maeno, H. Hashimoto, K. Yoshida, S. Nishizaki, T. Fujita, J. G. Bednorz, and F. Lichtenberg, Superconductivity in a layered perovskite without copper, Nature (London) **372**, 532 (1994).
[4] K. Takada, H. Sakurai, E. Takayama-Muromachi, F. Izumi, R. A. Dilanian, and T. Sasaki, Superconductivity in two-dimensional CoO_2 layers, Nature (London) **422**, 53 (2003).
[5] D. Li, K. Lee, B. Y. Wang, M. Osada, S. Crossley, H. R. Lee, Y. Cui, Y. Hikita, and H. Y. Hwang, Superconductivity in an infinite-layer nickelate, Nature (London) **572**, 624 (2019).
[6] H. Sun, M. Huo, X. Hu, J. Li, Z. Liu, Y. Han, L. Tang, Z. Mao, P. Yang, B. Wang, J. Cheng, D.-X. Yao, G.-M. Zhang, and M. Wang, Signatures of superconductivity near 80K in a nickelate under high pressure, Nature (London) **621**, 493 (2023).
[7] Z. Luo, X. Hu, M. Wang, W. Wú, and D.-X. Yao, Bilayer two-orbital model of $La_3Ni_2O_7$ under pressure, Phys. Rev. Lett. **131**, 126001 (2023).
[8] Y. Kamihara, T. Watanabe, M. Hirano, and H. Hosono, Iron-Based layered superconductor $La[O_{1-x}F_x]FeAs$

($x = 0.05$–0.12) with $T_c = 26$ K, J. Am. Chem. Soc. **130**, 3296 (2008).

[9] G. R. Stewart, Superconductivity in iron compounds, Rev. Mod. Phys. **83**, 1589 (2011).

[10] C. Castellani, C. R. Natoli, and J. Ranninger, Magnetic structure of V_2O_3 in the insulating phase, Phys. Rev. B **18**, 4945 (1978).

[11] W.-S. Wang, Y.-Y. Xiang, Q.-H. Wang, F. Wang, F. Yang, and D.-H. Lee, Functional renormalization group and variational Monte Carlo studies of the electronic instabilities in graphene near 1/4 doping, Phys. Rev. B **85**, 035414 (2012).

[12] Y.-Y. Xiang, F. Wang, D. Wang, Q.-H. Wang, and D.-H. Lee, High-temperature superconductivity at the FeSe/$SrTiO_3$ interface, Phys. Rev. B **86**, 134508 (2012).

[13] C. Honerkamp, M. Salmhofer, N. Furukawa, and T. M. Rice, Breakdown of the Landau-Fermi liquid in two dimensions due to umklapp scattering, Phys. Rev. B **63**, 035109 (2001).

[14] C. Honerkamp, D. Rohe, S. Andergassen, and T. Enss, Interaction flow method for many-fermion systems, Phys. Rev. B **70**, 235115 (2004).

[15] W. Metzner, M. Salmhofer, C. Honerkamp, V. Meden, and K. Schönhammer, Functional renormalization group approach to correlated fermion systems, Rev. Mod. Phys. **84**, 299 (2012).

[16] H. Yamase, A. Eberlein, and W. Metzner, Coexistence of incommensurate magnetism and superconductivity in the two-dimensional hubbard model, Phys. Rev. Lett. **116**, 096402 (2016).

[17] See Supplemental Material at http://link.aps.org/supplemental/10.1103/PhysRevB.108.L140505 for an introduction of the singular-mode functional renormalization group method (including Mandelstam parametrization and 1PI flow equations, singular scattering modes and order parameter analysis, benchmark of fermion bilinear truncation) and the Gutzwiller approximation of the effective Hamiltonian in the strong-coupling limit, which includes Refs. [31–35].

[18] W.-S. Wang, Z.-Z. Li, Y.-Y. Xiang, and Q.-H. Wang, Competing electronic orders on kagome lattices at Van Hove filling, Phys. Rev. B **87**, 115135 (2013).

[19] Q.-K. Tang, L. Yang, D. Wang, F.-C. Zhang, and Q.-H. Wang, Spin-triplet f-wave pairing in twisted bilayer graphene near 1/4-filling, Phys. Rev. B **99**, 094521 (2019).

[20] W. Kohn and J. M. Luttinger, New Mechanism for Superconductivity, Phys. Rev. Lett. **15**, 524 (1965).

[21] A. Chubukov, Pairing mechanism in Fe-based superconductors, Annu. Rev. Condens. Matter Phys. **3**, 57 (2012).

[22] H. Zhai, F. Wang, and D.-H. Lee, Antiferromagnetically driven electronic correlations in iron pnictides and cuprates, Phys. Rev. B **80**, 064517 (2009).

[23] T. A. Maier and D. J. Scalapino, Pair structure and the pairing interaction in a bilayer Hubbard model for unconventional superconductivity, Phys. Rev. B **84**, 180513(R) (2011).

[24] M. Nakata, D. Ogura, H. Usui, and K. Kuroki, Finite-energy spin fluctuations as a pairing glue in systems with coexisting electron and hole bands, Phys. Rev. B **95**, 214509 (2017).

[25] A. Kreisel, B. M. Andersen, A. T. Rømer, I. M. Eremin, and F. Lechermann, Superconducting instabilities in strongly correlated infinite-layer nickelates, Phys. Rev. Lett. **129**, 077002 (2022).

[26] D. J. Scalapino, A common thread: The pairing interaction for unconventional superconductors, Rev. Mod. Phys. **84**, 1383 (2012).

[27] F. C. Zhang, C. Gros, T. M. Rice, and H. Shiba, A renormalised Hamiltonian approach to a resonant valence bond wavefunction, Supercond. Sci. Technol. **1**, 36 (1988).

[28] Q.-H. Wang, Z. D. Wang, Y. Chen, and F. C. Zhang, Unrestricted renormalized mean field theory of strongly correlated electron systems, Phys. Rev. B **73**, 092507 (2006).

[29] Y. Zhang, L.-F. Lin, A. Moreo, and E. Dagotto, Electronic structure, orbital-selective behavior, and magnetic tendencies in the bilayer nickelate superconductor $La_3Ni_2O_7$ under pressure, arXiv:2306.03231.

[30] M. Yao, D. Wang, and Q.-H. Wang, Determinant quantum Monte Carlo for the half-filled Hubbard model with nonlocal density-density interactions, Phys. Rev. B **106**, 195121 (2022).

[31] J. Berges, N. Tetradis, and C. Wetterich, Non-perturbative renormalization flow in quantum field theory and statistical physics, Phys. Rep. **363**, 223 (2002).

[32] N. Dupuis, L. Canet, A. Eichhorn, W. Metzner, J. M. Pawlowski, M. Tissier, and N. Wschebor, The nonperturbative functional renormalization group and its applications, Phys. Rep. **910**, 1 (2021).

[33] P. Kopietz, L. Bartosch, and F. Schütz, *Introduction to the Functional Renormalization Group* (Springer, Berlin, 2010).

[34] M. C. Gutzwiller, Effect of correlation on the ferromagnetism of transition metals, Phys. Rev. Lett. **10**, 159 (1963).

[35] S.-Y. Wang, D. Wang, and Q.-H. Wang, Transition from band insulator to Mott insulator and formation of local moment in the half-filled ionic SU(N) Hubbard model, Phys. Rev. B **106**, 245113 (2022).